Biochimica et Biophysica Acta 1840 (2014) 3393–3403

Contents lists available at ScienceDirect

Biochimica et Biophysica Acta

journal homepage: www.elsevier.com/locate/bbagen

Diatomite biosilica nanocarriers for siRNA transport inside cancer cells

Ilaria Rea [a,*], Nicola M. Martucci [b], Luca De Stefano [a], Immacolata Ruggiero [b], Monica Terracciano [a,c], Principia Dardano [a], Nunzia Migliaccio [b], Paolo Arcari [b], Rosarita Taté [d], Ivo Rendina [a], Annalisa Lamberti [b]

[a] Institute for Microelectronics and Microsystems, National Council of Research, Naples, Italy
[b] Department of Molecular Medicine and Medical Biotechnology, University of Naples Federico II, Naples, Italy
[c] Department of Pharmacy, University of Naples Federico II, Naples, Italy
[d] Institute of Genetics and Biophysics, National Council of Research, Naples, Italy

ARTICLE INFO

Article history:
Received 4 April 2014
Received in revised form 3 September 2014
Accepted 5 September 2014
Available online 16 September 2014

Keywords:
Diatomite
Porous material
Surface modification
Photoluminescence
Nanovector
Drug delivery

ABSTRACT

Background: Diatomite is a natural porous biomaterial of sedimentary origin, formed by fragments of diatom siliceous skeletons, called "frustules". Due to large availability in many areas of the world, chemical stability, and non-toxicity, these fossil structures have been widespread used in lot of industrial applications, such as food production, water extracting agent, production of cosmetics and pharmaceutics. However, diatomite is surprisingly still rarely used in biomedical applications. In this work, we exploit diatomite nanoparticles for small interfering ribonucleic acid (siRNA) transport inside human epidermoid cancer cells (H1355).
Methods: Morphology and composition of diatomite microfrustules (average size lower than 40 μm) are investigated by scanning electron microscopy equipped by energy dispersive X-ray spectroscopy, Fourier transform infrared analysis, and photoluminescence measurements. Nanometric porous particles (average size lower than 450 nm) are obtained by mechanical crushing, sonication, and filtering of micrometric frustules. siRNA bioconjugation is performed on both micrometric and nanometric fragments by silanization.
Results: In-vitro experiments show very low toxicity on exposure of the cells to diatomite nanoparticle concentration up to 300 μg/ml for 72 h. Confocal microscopy imaging performed on cancer cells incubated with siRNA conjugated nanoparticles demonstrates a cytoplasmatic localization of vectors. Gene silencing by delivered siRNA is also demonstrated.
Conclusion: Our studies endorse diatomite nanoparticles as non-toxic nanocarriers for siRNA transport in cancer cells.
General significance: siRNA is a powerful molecular tool for cancer treatment but its delivery is inefficient due to the difficulty to penetrate the cell membrane. siRNA-diatomite nanoconjugate may be well suited for delivery of therapeutic to cancer cells.

1. Introduction

Diatomaceous earth, also known as diatomite, is a fossil material of sedimentary origin, formed over centuries by siliceous skeleton (called "frustule") of aquatic unicellular microalgae, the diatoms, deposited on bottom of lakes or present in marine environments. Diatomite morphology can be very complex due to the presence of diatom frustules with different sizes (ranging from 2 μm to 2 mm) and shapes. The structure is highly porous and characterized by a large specific surface area up to 200 m^2/g [1]. The main constituent of diatomite is amorphous silica, although it can contain impurities such as organic components and metallic oxides (MgO, Al_2O_3, Fe_2O_3) coming from environment [1,2]. Different strategies, including calcination processes and hot acid treatments, have been developed to remove impurities from frustules [3,4].

Due to large availability in many areas of the world, chemical stability, and non-toxicity, this fossil material has been widespread used in lot of industrial applications, such as food production, water extracting agent, production of cosmetics and pharmaceutics [5–8].

Recently, diatom frustules have been exploited as an innovative platform in several biotechnological applications [9,10]. In fact, the silica surface of diatoms, covered by reactive silanol (Si – OH) groups, can be modified with functional reactive groups (– NH_2, – COOH, – SH, – CHO) for the immobilization of biomolecular probes (DNA, antibodies, enzymes) [11]. Moreover, the porous structure allows the binding 0of a large amount of bioprobe molecules with respect to a flat surface, thus increasing sensitivity of biosensing. In recent works, we reported the chemical modification of marine diatom frustules with antibody as highly-selective bioprobe. The antibody–antigen molecular recognition was investigated by means of photoluminescence and fluorescence microscopy [12,13].

Although diatomite, differently from diatom frustules, is a cheaper material produced in tons by mining industry, it is surprisingly still

* Corresponding author. Tel.: +39 0816132594; fax: +39 0816132598.
E-mail address: ilaria.rea@na.imm.cnr.it (I. Rea).

http://dx.doi.org/10.1016/j.bbagen.2014.09.009
0304-4165/

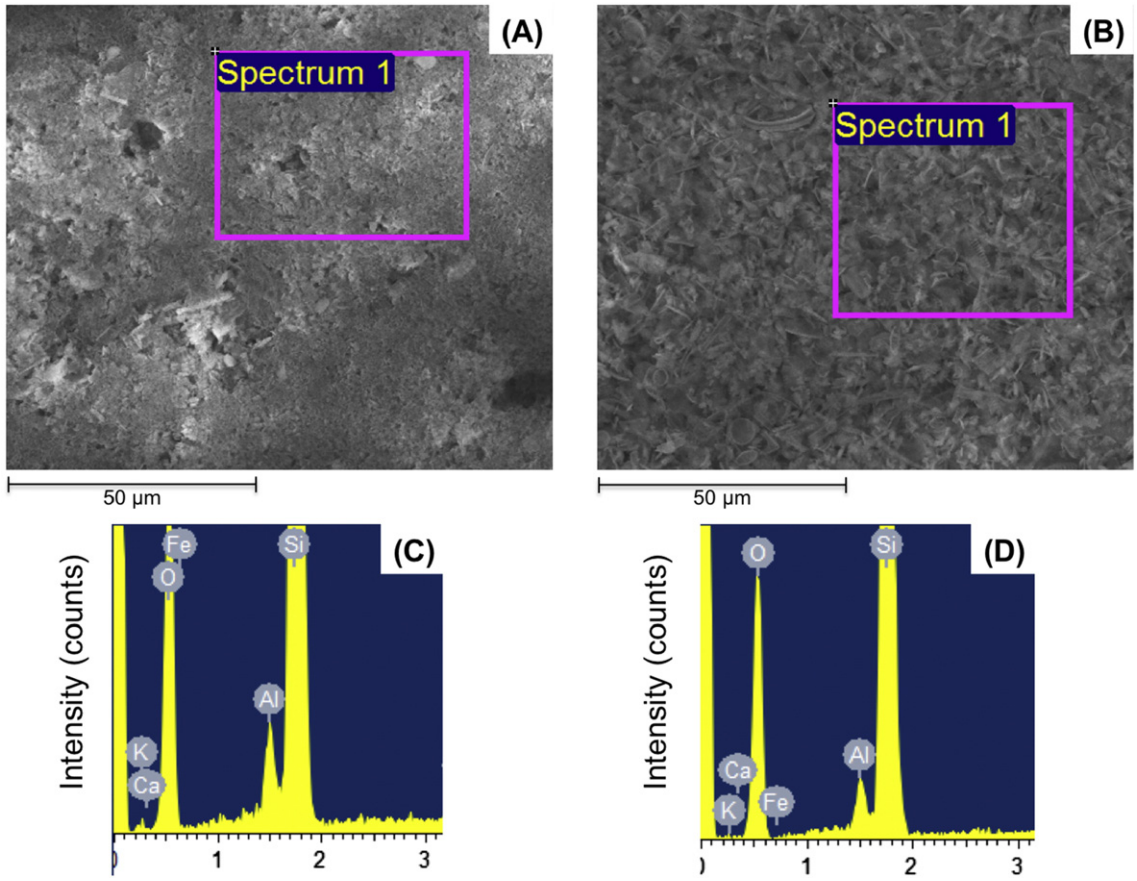

Fig. 1. SEM images of diatomite deposited on silicon before (A) and after (B) purification treatments; corresponding EDS graphs (C–D).

scarcely used in biomedical applications. Recent pioneering papers demonstrated the use of diatomite as microcapsules for oral drug delivery [14,15]. In our previous work, we presented a preliminary study on silica nanovectors made from fragments of diatomite [16]. However, the results reported in these works require further investigations to clarify the potential of this intriguing natural material.

In this work, porous diatomite nanocarriers, with an average diameter less than 450 nm, were bioconjugated with small interfering ribonucleic acid (siRNA) in order to test their drug delivery capability. As a matter of fact, siRNA is a powerful approach for silencing genes associated with a variety of pathologic conditions but its systemic delivery is inefficient due to the difficulty to penetrate the cell membrane [17,18]; its conjugation to nanovectors (including liposomes, gold and magnetic nanoparticles, quantum dots) is one of the possible strategies developed to overcome this challenging problem [19,20]. In particular, we have investigated cytotoxicity of diatomite nanoparticles and examined their ability to transport siRNA inside cancer cells and to silence gene expression. The results, compared with those reported in literature on standard systems [21,22], encourage the use of diatomite nanoparticles as drug carriers.

Table 1
Chemical composition of frustules before and after purification treatments.

Compounds	Before purification treatment (%)	After purification treatment (%)
SiO_2	92.1	94.6
Al_2O_3	3.3	2.7
K_2O	1.0	0.8
CaO	1.8	0.9
Fe_2O_3	1.8	1.0

2. Materials and methods

2.1. Materials

Calcined diatomite was obtained by DEREF Spa (Italy); 3-(4,5-dimethythiazol-2-yl)-2,5-diphenyl tetrazolium bromide (MTT), (3-aminopropyl)triethoxysilane (APTES), Tris(2-carboxyethyl)phosphine hydrochloride (TCEP) and H_2SO_4 were purchased from Sigma-Aldrich (MO, USA). Phosphate buffered saline (PBS) was purchased from GIBCO (CA, USA). N-(γ-Maleimidobutyryloxy) sulfosuccinimide ester (Sulfo-GMBS), on target plus smart pool human GAPDH (siRNA GAPDH), on target plus control pool non-targeting pool (siRNA scramble, SCR) and siGLO RISC-Free control siRNA (siGLO RNAi), chemically modified to impair processing and uptake by RISC, were from Thermo Scientific (MMedical, Milan, Italy). Synthesis of poly D-Arg peptide (sequence RRRRRRRRC) and non polar homopeptide was performed by Proteogenix (FR). HCl was purchased from Romil (UK). Absolute ethanol, Tris-(hydroxymethyl)aminomethane, NaCl and H_2O_2 were purchased from Carlo Erba (IT). Rabbit anti-GAPDH polyclonal antibody was purchased from Cell Signaling Technology Inc. (MA, USA). Rabbit anti-β-tubulin polyclonal antibody and goat anti-rabbit immunoglobulin conjugated to horseradish peroxidase were from Santa Cruz Biotechnology (CA, USA).

2.2. Diatomite purification treatments

5 g of diatomite powder was dissolved in 250 ml of absolute ethanol and sonicated for 5 h in order to break up macroscopic aggregates. The dispersion was filtered through a nylon net filter with pore size of 41 µm (Millipore). Natural diatomite needs purification treatments in order to remove organic and inorganic contaminants [1,3]. To this aim, diatomite

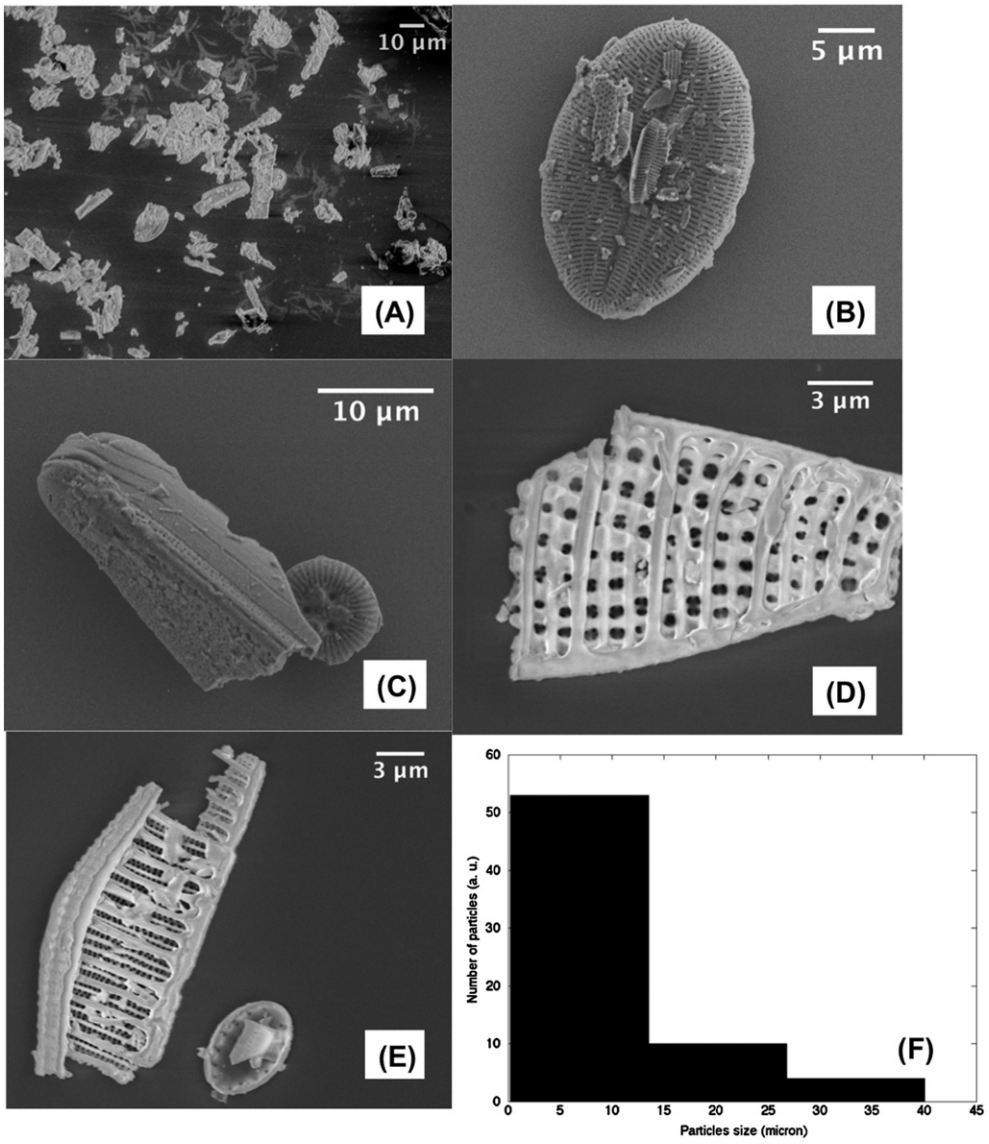

Fig. 2. SEM images of purified diatomite structures (A–E) and particles size histogram (F) calculated from (A).

dispersion was centrifuged and the pellet was suspended in piranha solution (2 M H_2SO_4, 10% H_2O_2) for 30 min at 80 °C. Dispersion was then centrifuged for 30 min at 15,000 ×*g* and supernatant was removed. Diatomite was washed twice with deionized water. Subsequently, 5.0 M HCl solution was added to diatomite and incubated overnight at 80 °C. After HCl incubation, diatomite dispersion was centrifuged for 30 min and supernatant was removed. Pellet was washed twice with deionized water that removed excess of HCl. The effects of purification treatments have been evaluated by scanning electron microscopy with X-ray micro-analysis, Fourier transform infrared spectroscopy and photoluminescence analysis, once diatomite samples have been deposited on silicon (p-type, 0.003 ohm cm resistivity, <100> oriented, 500 μm thick) chips of about 1 cm × 1 cm.

2.3. Scanning electron microscopy

Morphology and chemical composition of diatomite, before and after purification treatments, were investigated by scanning electron microscopy (SEM) equipped with energy dispersive X-ray spectroscopy (EDS) (Fei, Quanta 200 FEG). Diatomite samples were deposited on crystalline silicon substrates mounted on a double-faced conductive adhesive tape. Images were acquired at 5 kV accelerating voltage and 30 μm wide aperture.

2.4. Fourier transform infrared spectroscopy

Surface chemical composition of diatomite has been investigated by Fourier transform infrared spectroscopy (FTIR). FTIR spectra have been recorded by a Nicolet Continuμm XL (Thermo Scientific) equipped with a microscope; measurements have been performed in reflection mode on an area of 100 × 100 μm^2. The number of scans was set to 64. Spectra were collected in the range of 1600–500 cm^{-1} with a resolution of 2 cm^{-1}. The spectrum of bare silicon acquired in ambient air was used as background.

2.5. Steady-state photoluminescence

Steady-state photoluminescence (PL) spectra were excited by a continuous wave He–Cd laser at 325 nm (KIMMON Laser System). PL was collected at normal incidence to the surface of samples through a fiber, dispersed in a spectrometer (Princeton Instruments, SpectraPro 300i), and detected using a Peltier cooled charge coupled device (CCD)

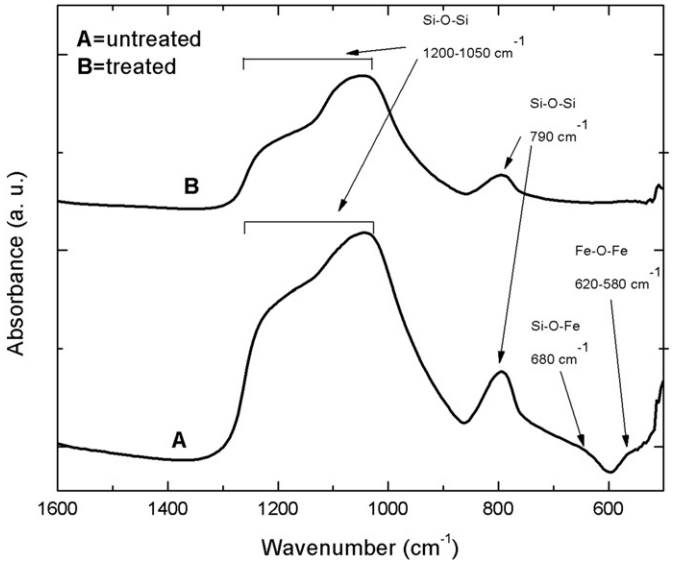

Fig. 3. FTIR spectra of untreated diatomite (A) and of diatomite after purification treatments (B).

camera (PIXIS 100F). A long pass filter with a nominal cut-on wavelength of 365 nm was used to remove the laser line at monochromator inlet.

2.6. Diatomite chemical functionalization

After purification treatments, diatomite surface was amino-modified by incubation with a 5% (*v*/*v*) APTES solution in absolute ethanol, following typical silanization processes [23,24]. Briefly, the reaction was performed for 1 h at room temperature with stirring in dark condition. Dispersion was then centrifuged for 30 min at 15,000 ×*g* and supernatant was removed. The functionalized diatomite was washed twice with absolute ethanol; the collected pellet was incubated for 10 min at 100 °C (curing process). After incubation, the sample was resuspended and washed twice with absolute ethanol and then twice with PBS 1X pH 7.4. APTES-functionalized diatomite was incubated with 20 mM Sulfo-GMBS in PBS for 1 h with stirring at room temperature. Subsequently, the sample was washed twince with PBS 1X to remove Sulfo-GMBS excess

2.7. Peptide/siRNA complex

The relative concentrations of peptide and siRNA required to form a stable complex have been investigated by incubating 50 pmol of siRNA with different amounts of arginine peptide for 2 h at room temperature in PBS, with a peptide/siRNA charge ratio ranging from 0 to 20. The ratio between peptide (NH_3^+) and siRNA (PO_4^-) was defined as the nitrogen/phosphate (N/P) ratio. Peptide/siRNA complexes were analyzed by electrophoretic mobility shift assay (EMSA) on a 20% polyacrylamide gel in TAE (40 mM Tris acetate/2 mM EDTA) buffer at 100 V for 70 min, followed by staining with ethidium bromide (EtBr) for 20 min. In addition, the stability of siRNA to nuclease was evaluated in the absence and presence of poly-Arg peptide. The samples were incubated in PBS for 30 min in the presence of human pancreatic ribonuclease, gently provided by Prof. De Lorenzo, that is able to degrade double-strand RNA [25]. Samples were then analyzed by EMSA.

Finally, in order to assess the optimal peptide concentration, Sulfo-GMBS modified diatomite was incubated with increasing concentrations (75, 150, 300 μM) of labeled peptide and fluorescence intensity was analyzed (data not shown).

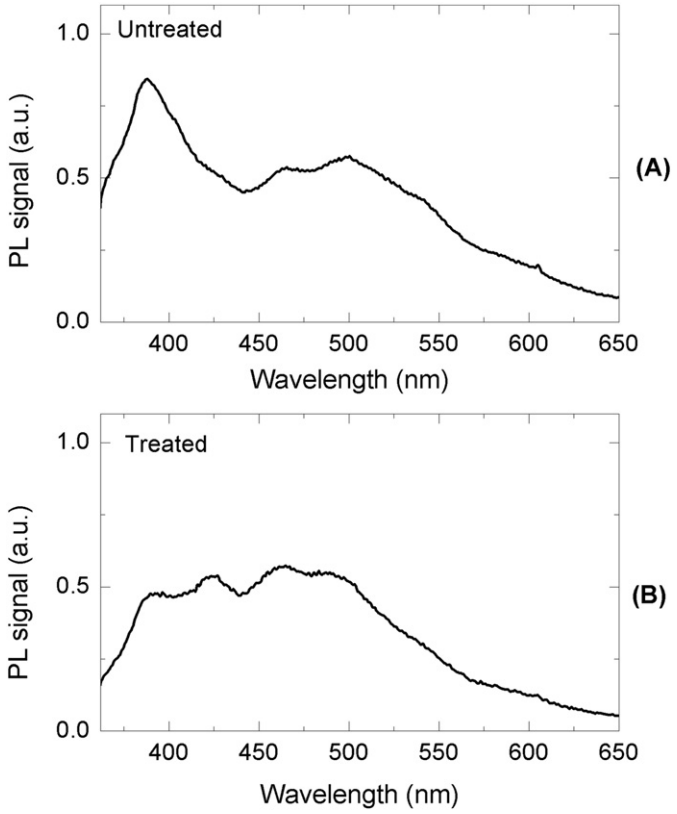

Fig. 4. Photoluminescence spectra of untreated diatomite (A) and diatomite after piranha and HCl treatments (B).

2.8. siRNA loading

0.5 mg of sulfo-GMBS modified diatomite was incubated with the complex formed by peptide and siRNA for 1 h at room temperature in dark condition. Complex was obtained by mixing 150 μM peptide with 7.5 μM siRNA (molar ratio 20:1) in the presence of a 10-fold molar excess with respect to the peptide concentration of a reducing agent, Tris(2-carboxyethyl)phosphine hydrochloride (TCEP), in PBS at room temperature for 2 h in dark condition [26,27]. Subsequently, diatomite suspension was centrifuged and the pellet was collected and washed twice with PBS 1X. The siRNA loaded was about 0.7 pmol per 1.0 μg of diatomite, as determined by UV reading at 260 nm.

2.9. Fluorescence microscopy

Fluorescence of diatomite modified with Dy547 labeled siRNA (siRNA*) was investigated by means of Leica Z16 APO fluorescence macroscope equipped with a camera Leica DFC300, using an optics constituted by a 515–560 nm band-pass excitation filter, a 580 nm dichromatic mirror, and a 590 nm suppression filter. Analysis was performed on diatomite samples deposited on silicon substrates. Fluorescence values reported in the work are the average of three different measurements.

2.10. siRNA release profile

The siRNA release profile was performed by suspending siRNA* modified diatomite in 20 mM TrisHCl pH 7.5 and 20 mM NaCl at room temperature and then monitoring the fluorescence intensity in the supernatant and in diatomite at different time points. Images were acquired on an Axiovert 40 CFL Zeiss and fluorescence intensity was analyzed by using ImageJ software (http://imagej.nih.gov/ij/).

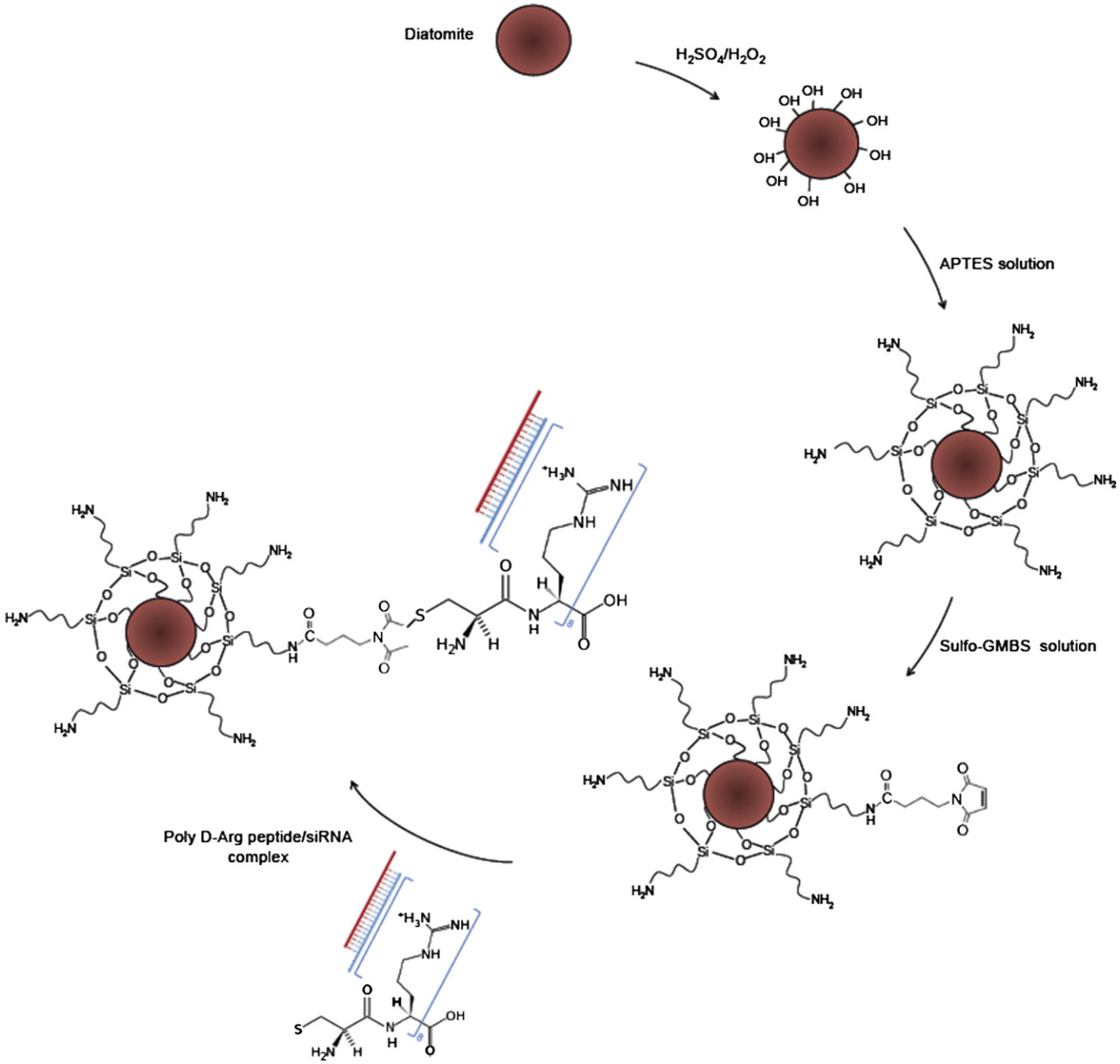

Fig. 5. Functionalization scheme of diatomite frustules with labeled siRNA (siRNA*).

2.11. Fabrication and functionalization of diatomite nanoparticles

Purified diatomite frustules (following procedure described in Section 2.2) were re-dispersed in ethanol and further filtered using 0.45 μm syringe filters (Millipore-Millex). Dispersion of diatomite nanoparticles was centrifuged at 15,000 ×*g* for 30 min, and the supernatant was removed. Nanoparticles were loaded with siRNA following procedure described in Sections 2.6 and 2.8.

2.12. Cell culture

The human lung epidermoid carcinoma cell line (H1355), obtained from the American Type Tissue Collection (Rockville, MD, USA), was grown in RPMI 1640 (GIBCO) medium supplemented with 10% heat inactivated FBS (GIBCO), 100 U/ml penicillin, 100 mg/ml streptomycin, and 1% L-glutamine at 37 °C in a 5% CO_2 atmosphere. H1355 cell line was used as *in vitro* cell model to test the drug delivery system.

2.13. Cell viability assay

Cells were seeded into 96-well microtiter plates (BD Falcon, USA) at the density of 30×10^3 cells/well and allowed to attach for 24 h. After incubation, the medium was removed and a fresh cell growth medium was added (100 μl/well). Diatomite nanoparticles at concentrations of 0, 20, 50, 100, 200, and 300 μg/ml were added into different wells in triplicate and incubated with cells for 24, 48, and 72 h. After treatment, the cell viability was assessed using MTT assay. 10 μl of a 5 mg/ml MTT solution in RPMI 1640 no phenol red (Sigma) was added to each well. Plates were then incubated under cell culture conditions for 3 h. Subsequently, 100 μl of MTT solvent (HCl 0.1 N in isopropanol) was added to each well and incubated for 1 h at room temperature with stirring to

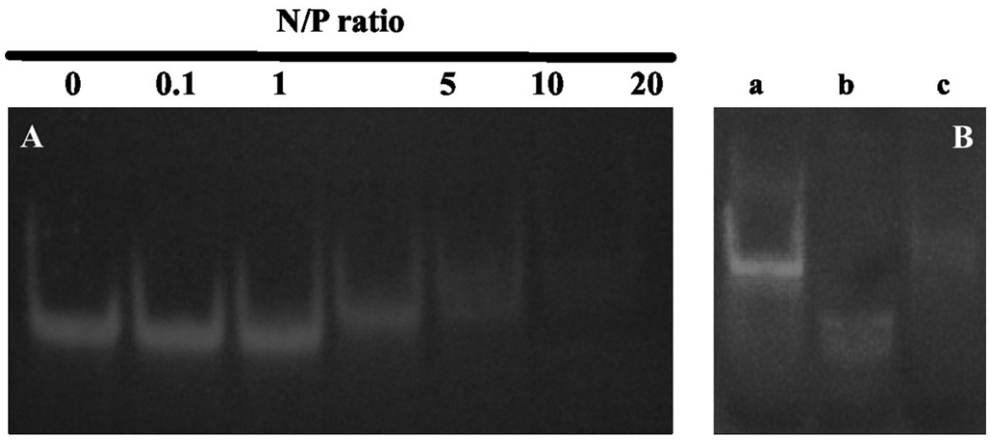

Fig. 6. (A) Poly D-Arg peptide (N) and siRNA (P) were incubated at different molar ratios (range 0–20, as indicated above each lane) and the formed complex was analyzed by gel shift. (B) Effect of HP-RNase on siRNA degradation; siRNA alone (lane a), siRNA incubated with HP-RNase in absence (lane b) or in the presence (lane c) of poly D-Arg peptide.

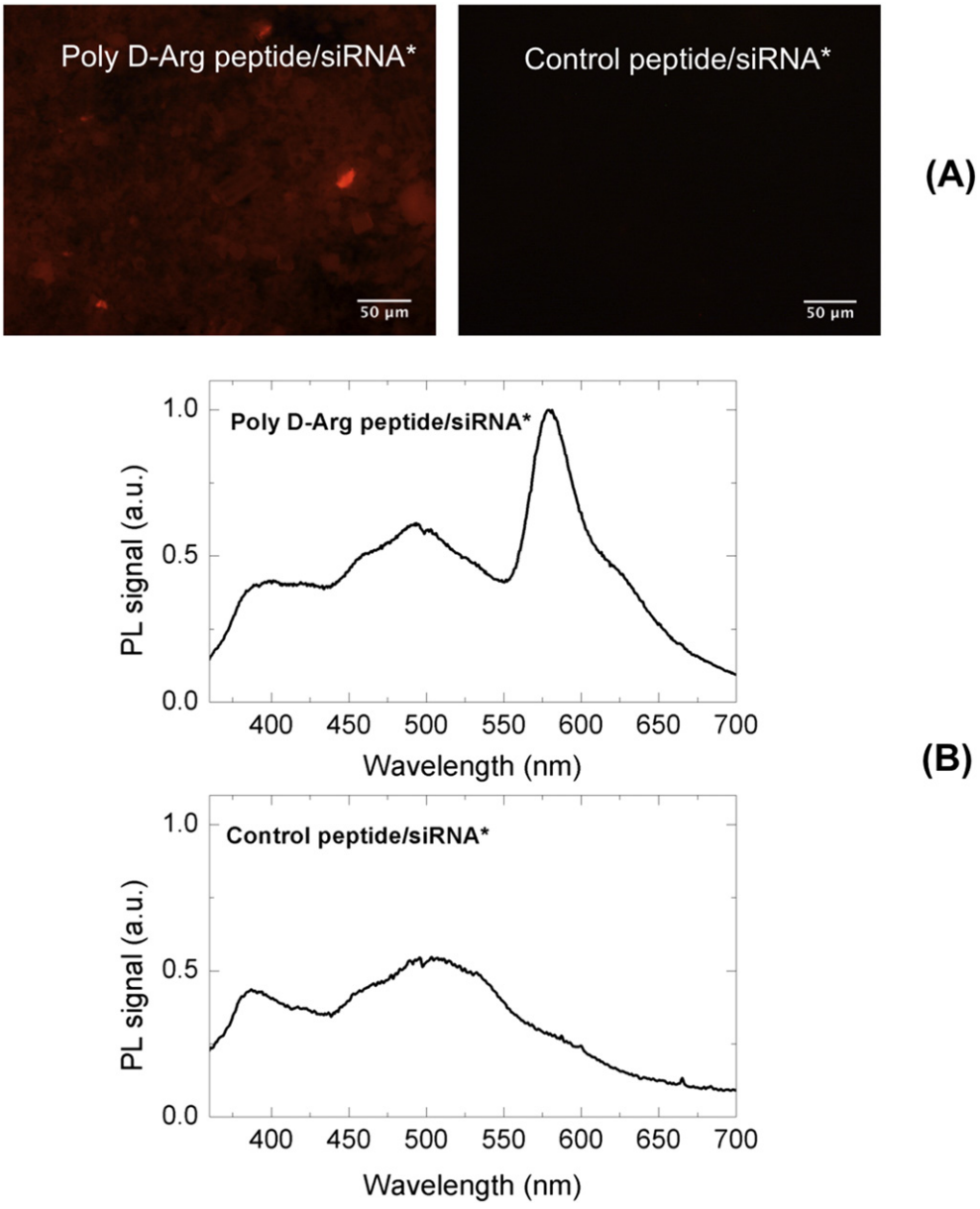

Fig. 7. (A) Fluorescence microscopy images of diatomite modified with Poly D-Arg peptide/siRNA* (left image) and with a control peptide/siRNA* (right image); (B) corresponding photoluminescence spectra.

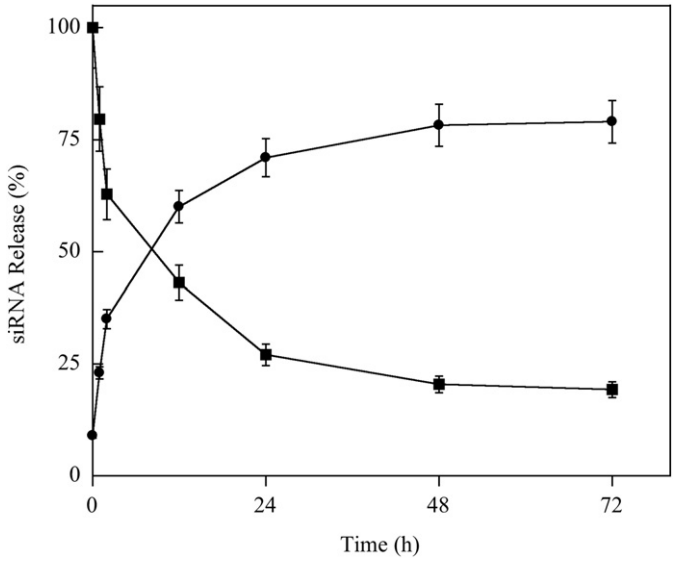

Fig. 8. Fluorescent labeled siRNA bound to DNPs (DNPs–siRNA*) was incubated in 20 mM Tris–HCl and 20 mM NaCl, pH 7.5 at 37 °C and at time intervals the fluorescence intensity was measured in the sample supernatant (●) and diatomite (■).

dissolve the formazan crystals. Absorbance of each sample was detected by Microplate Reader 680 (Biorad) at 570 nm.

2.14. Confocal microscopy imaging of nanoparticles internalization

Cells (50×10^3/coverslip) were plated on 10 mm glass coverslips placed on the bottom of 24-well plate, allowed to attach for 24 h under normal cell culture conditions and then incubated with siRNA* modified diatomite nanoparticles (300 μg/ml) for 18 h. Cells were washed with PBS, fixed in 4% formaldehyde for 30 min, washed 3 times with PBS, and stained with membrane stain WGA-Alexa Fluor 488 Conjugate (Invitrogen, Carlslab, CA) according to the manufacturer's instructions. Cell nuclei were then stained with Hoechst 33342 (Invitrogen, Carlslab, CA). Images were acquired at 63× magnification on a LSM710 confocal fluorescence microscope (Carl Zeiss Inc., Peabody, MA) with the appropriate filters.

2.15. Gene knockdown

Cells (150×10^3/well) were seeded into six-well plates 24 h before incubation with GAPDH and non-targeting (SCR) siRNA modified diatomite nanoparticles (100 pmol siRNA/140 μg diatomite) in RPMI1640. After 72 h of incubation, the cells were used for Western blot analysis. Transfection with 100 pmol GAPDH and SCR siRNAs by using Lipofectamine 2000 (LF2000) according to the manufacturer's instructions (Invitrogen) was used as comparison.

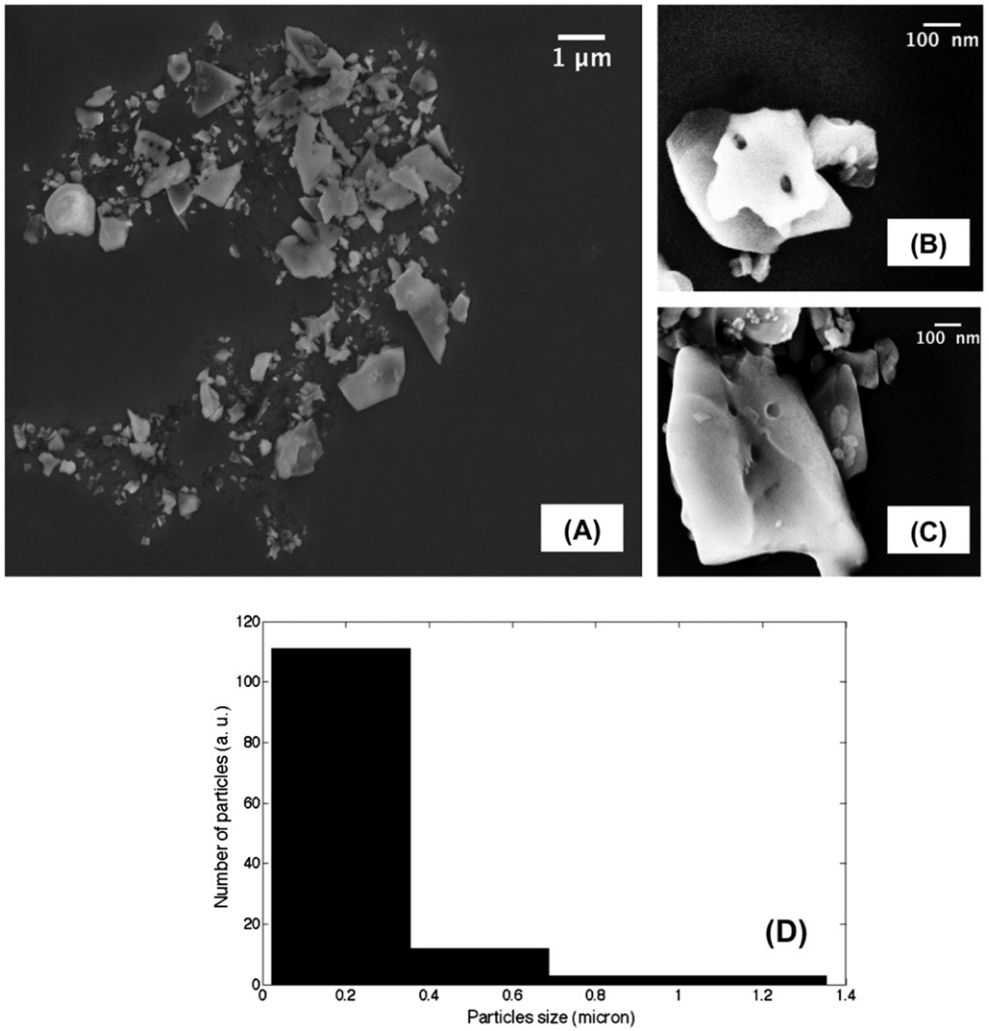

Fig. 9. SEM images of diatomite nanoparticles (A–C) and particles size histogram (D) calculated from (A).

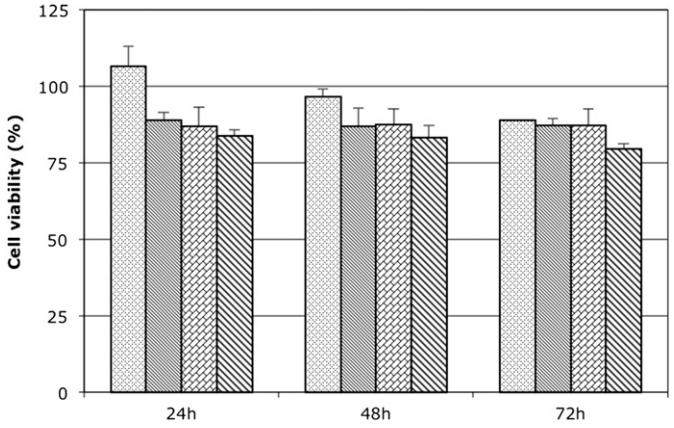

Fig. 10. Cytotoxicity assessment of diatomite nanoparticles using MTT assay. Cell viability of H1355 cells treated with 20 □, 100 ▧, 200 ▨ and 300 ▩ μg/ml of nanoparticles for 24, 48 and 72 h at 37 °C. Data represent the mean ± s.d. ($n = 3$). Cell viability was expressed as the percentage of viable cells compared with cells cultured without nanoparticles as control (100%).

H1355 cells were scraped, washed twice in cold phosphate-buffered saline (PBS), and resuspended in 20–40 ml of lysis buffer (50 mM Tris–HCl pH 7.4, 1% NP40, 0.25% sodium deoxycholate, 150 mM NaCl, 1 mg/ml aprotinin, leupeptin, pepstatin, 1 mM Na_3VO_4, 1 mM NaF) for 30 min on ice and centrifuged at 14,000 ×*g* for 20 min at 4 °C. Protein concentration was determined by a modified Bradford method, using the Bio-Rad protein assay and compared with BSA standard curve. Cytosolic proteins (10 μg) were separated by SDS-PAGE, electrotransferred to nitrocellulose and reacted with the different antibodies. Blots were then developed using enhanced chemiluminescence detection reagents (SuperSignal West Pico, Pierce) and exposed to X-ray film. All films were scanned for densitometric analysis by using ImageJ 1.41o software (http://imagej.nih.gov/ij/).

3. Results and discussion

3.1. Characterization of diatomite microparticles

Natural diatomite is generally contaminated by organic residues and inorganic oxides [1,2]. Biomedical applications require strong purification treatments of microshells in order to obtain pure silica as safe and biocompatible material. Fig. 1 shows SEM images of diatomite frustules deposited on silicon support, before (A) and after (B) purification treatments in strong hot acids.

Before purifications, the features of diatomite frustules are completely masked by the presence of many impurities on their surface; frustules with different shapes can be distinguished after removal of impurities. EDS spectra showed changes in chemical composition of the samples: after cleaning treatments, the intensities of peaks corresponding to calcium, iron and aluminum decreased, whereas the silica peak increased (Fig. 1C and D). Detailed chemical composition of diatomite before and after purification is summarized in Table 1.

A more accurate morphological analysis performed on purified samples is reported in Fig. 2(A–E) showing SEM images of different deep structures present in the diatomite used in this study.

The matter was composed by a mixture of fragments with circular, elliptical, elongated, and squared shape. The histogram of particle size, reported in Fig. 2(E) and calculated from (A), showed dimension distribution ranging from few microns up to about 40 μm with a maximum near to 7 μm. From these images, it was also possible to appreciate the porous morphology of diatomite useful for drug loading.

The purification procedures have also been investigated by FTIR spectroscopy and photoluminescence analysis.

FTIR spectra of untreated (A) and purified (B) diatomite are shown in Fig. 3. In both spectra, the broad band at 1200–1050 cm^{-1} and the peak at 790 cm^{-1} due to the presence of Si – O – Si species are well evident [28]. These features are characteristic of diatomite silica framework. After treatment in acid solutions, the peak at 680 cm^{-1} and the band at 620–580 cm^{-1} related to Si – O – Fe and Fe – O – Fe bonds [28], respectively, disappeared due to the removal of metallic impurities from amorphous silica matrix.

Under UV excitation (325 nm), diatomite samples showed a blue photoluminescence, clearly visible by naked eye. Even if the origin of this emission is not completely clear, it is commonly believed that it is mainly originated from surface defects including OH^- groups and oxygen vacancies [29]. Laser pumping generates excited electrons whose radiative decay produces photoluminescence emission.

Fig. 4 shows the comparison between photoluminescence spectra of diatomite before (A) and after (B) treatments. The untreated sample was characterized by a weak signal with three main features peaked at 390 nm (3.18 eV), 460 nm (2.7 eV), and 500 nm (2.48 eV).

After treatment, the peak at 390 nm became weaker, another peak at 423 nm (2.93 eV) appeared, while the feature at 500 nm shifted to

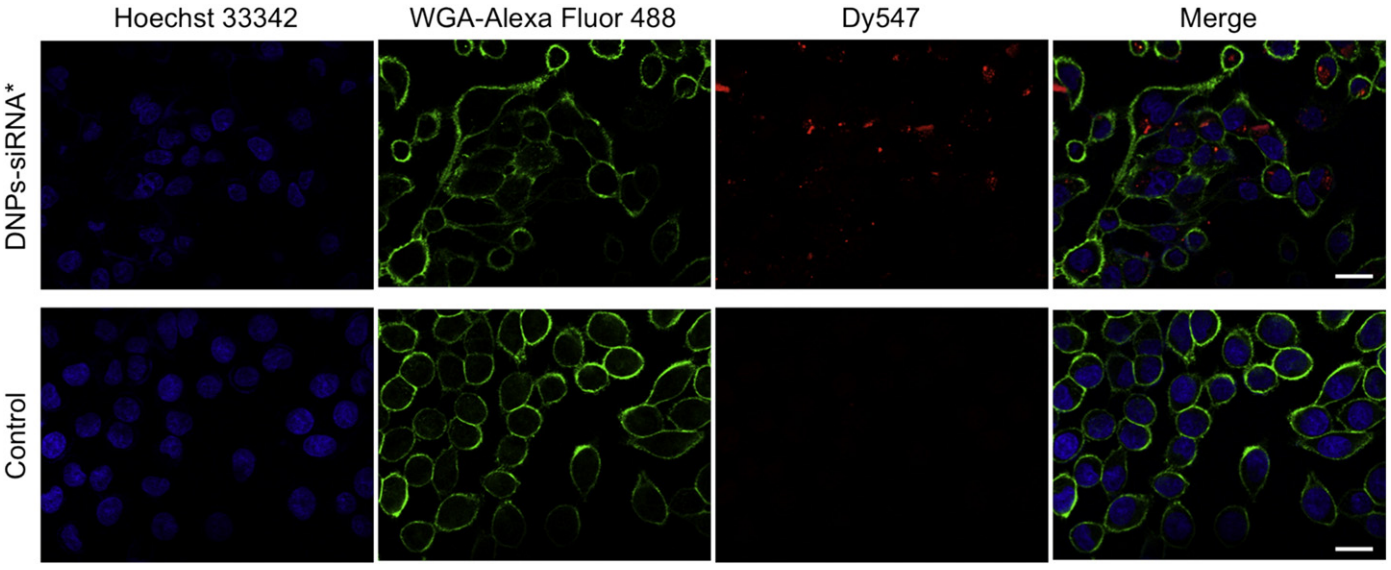

Fig. 11. Confocal microscopy on cells treated with siRNA* modified diatomite nanovectors (first line) and untreated cells as control (second line). Cell nuclei and membranes were stained with Hoechst 33342 and WGA-Alexa Fluor 488, respectively. siRNA was labeled with Dy547. Scale bar corresponds to 20 μm.

490 nm (2.53 eV). These modifications were due to the removal of metallic impurities from the frustule surface, accordingly to FTIR characterization. The absence of impurities significantly modified the photoluminescence signal changing reactions of energy transfer by surface radiative recombination.

3.2. Study of siRNA loading into diatomite microparticles and in vitro release

siRNA*, complexed with a poly D-Arg peptide, was loaded onto diatomite microparticles following the functionalization procedure sketched in Fig. 5. Briefly, APTES-functionalized diatomite reacts with sulfo-GMBS, a heterobifunctional cross linker reactive to amino groups at one end and to sulfhydryl groups at the other. The NHS ester reacts with the amino-modified diatomite surface as a nucleophile with release of the sulfo-NHS leaving group forming an amide bond. Peptide/siRNA* complex (molar ratio 20:1) was immobilized on the diatomite surface through the thioether bond between the sulfhydryl group of peptide cysteine residue and C – C bond of the maleimide ring of Sulfo-GMBS. A nonpolar homopeptide was used as control for aspecific interactions with siRNA.

The molar ratio peptide/siRNA* used in the functionalization procedure has been established by a gel shift assay, highlighting the complex electrostatic interaction as function of the positive peptide (NH_3^+)/ negative RNA (PO_4^-) charge ratios. siRNA (50 pmol) was mixed with arginine peptides at various N/P ratios (0–20). The results showed that the electrophoretic migration of RNA was retarded with an increasing ratio of peptide/RNA (Fig. 6(A)). The intensity of the siRNA band decreased as the N/P ratio increased. No siRNA band was observed at the N/P ratio of 20. This absence of migration was probably due to the complete neutralization of nucleic acid charge by the arginine peptide and/or formation of a large complex between the arginine and siRNA. These results strongly suggest that an arginine peptide made of 8 residues could be sufficient to form a complex with a siRNA.

In addition, the capability of the peptide/siRNA complex to protect siRNA from nuclease degradation was investigated. For this purpose, human pancreatic ribonuclease (HP-RNase) that is able to degrade double-strand RNA was used [25]. As shown in Fig. 6(B), siRNA was rapidly degraded by HP-RNase (lane b), while, when preincubated with peptide before adding RNase, no significant degradation was observed (lane c). Our data confirmed that a poly D-Arg peptide strongly interacts with siRNA forming a highly stable complex as previously reported [25,26]. Furthermore, the formation of the peptide/siRNA complex improved the siRNA stability protecting it from nuclease degradation [30].

Diatomite functionalization was evaluated by means of fluorescence microscopy and photoluminescence analysis. Fig. 7(A) shows the images of diatomite microfrustules incubated with poly D-Arg peptide/siRNA* (left image) and control peptide/siRNA* (right image). High red fluorescence (average intensity $= 27 \pm 2$) was well evident only using poly D-Arg peptide/siRNA*; conversely, diatomite incubated with control peptide/siRNA* appeared darker (average intensity $= 9 \pm 1$). The result was confirmed by PL measurements. PL spectra of diatomite functionalized with poly D-Arg peptide/siRNA* and control peptide/siRNA* are compared in Fig. 7(B). Only the sample functionalized with specific peptide was characterized by a strong PL peak at 575 nm due to the presence of labeled nucleic acid.

It was also investigated the capability of loaded diatomite to release in solution siRNA* by measuring the fluorescence intensity of both supernatant and diatomite as function of time (Fig. 8). siRNA was released into supernatant in two phases: an initial phase of 12 h (burst release), followed by slow and sustained release phase over 48–72 h. The fluorescence profile of diatomite showed an opposite trend. The slow siRNA release observed was probably due to the progressive weakening of the electrostatic interactions between peptide and nucleic acid.

3.3. Diatomite nanovectors: toxicity and internalization

A micrometric to nanometric reduction of diatomite average size is required in order to optimize their cell uptake. Nanovectors were obtained by mechanical crushing, sonication, and filtering of micrometric diatomite fragments. Purification treatments in hot acids were performed on micrometric frustules, before reduction to nanometric size. Morphology of diatomite nanoparticles was explored by scanning electron microscopy. SEM images of nanoparticles are reported in Fig. 9(A–C) together with particles size histogram, shown in Fig. 9(D) and calculated from (A). Morphological characterization revealed the presence of

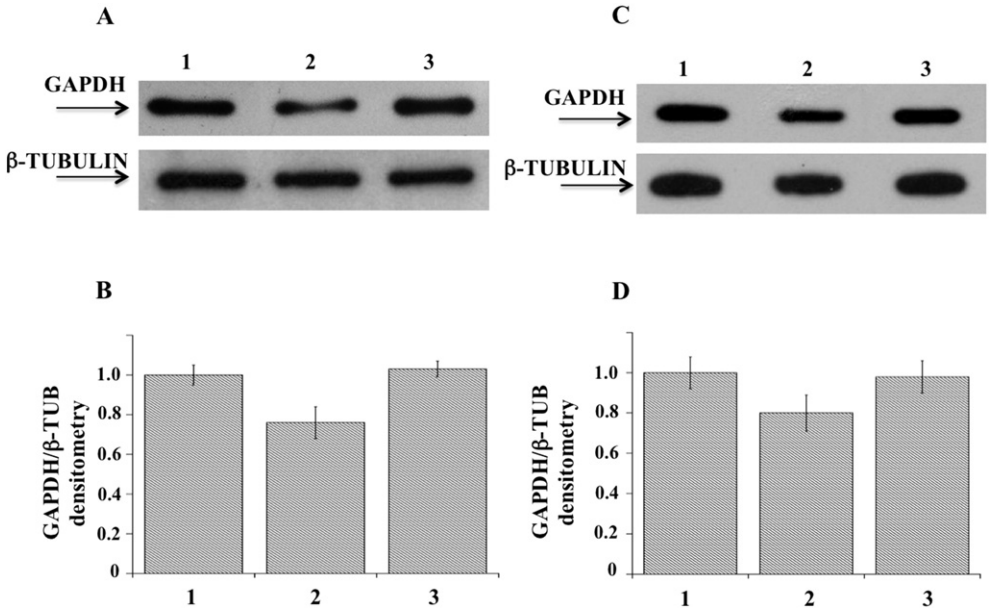

Fig. 12. (A) Immunoblotting analysis of GAPDH (upper gel) and of β-tubulin (lower gel) of protein expression in DNPs–siRNA treated cells. Lanes: 1) control cells; 2) DNPs–GAPDH–siRNA; 3) DNPs–SCR–siRNA. (B) Densitometric intensity band ratio of GAPDH and β-tubulin used as internal control. The intensities of the bands were expressed in arbitrary units. (C) Immunoblotting analysis of GAPDH (upper gel) and of β-tubulin (lower gel) protein expression in lipofectamine-siRNA transfected cells. Lanes: 1) control cells; 2) GAPDH–siRNA; and 3) SCR–siRNA. (D) Densitometric intensity band ratio of GAPDH and β-tubulin used as internal control. The intensities of bands were expressed in arbitrary units. Each measurement and Western blot was carried out in triplicate. Error bars indicate the maximum deviation from the mean value of two independent experiments.

diatomite fragments with different shape and size distribution, ranging from few nanometers to about 1 μm, with a maximum at 250 nm. Size polydispersivity could be reduced performing more filtration steps at 0.45 μm. This procedure would improve the quality of diatomite but introduce further loss of material. After nanometric size reduction, it is still possible to observe the porous structure of nanoparticles (Fig. 9(B–C)), characterized by pores of about 40 nm.

A critical issue for biomedical applications of new nanocarriers for drug delivery is the evaluation of their potential toxicity and biocompatibility [14,21,22]. *In vitro* cytotoxicity of DNPs was evaluated by MTT assay, a method based on the reduction of 3-(4,5-dimethythiazol-2-yl)-2,5-diphenyl tetrazolium bromide by cellular oxidoreductases of viable cells, that yield a crystalline blue formazan product. H1355 cells were incubated with different concentrations of diatomite nanoparticles for 24, 48 and 72 h. The results obtained are reported in Fig. 10.

The exposure of H1355 cells to increasing nanoparticle concentrations (20 μg/ml, 100 μg/ml, 200 μg/ml and 300 μg/ml) induced very low toxicity being the average viability of the cells slightly lower than 100%. This result also demonstrated that the irregular shape of diatomite nanoparticles did not influence cell growth and morphology. In conclusion, the MTT assay showed that H1355 cell viability was not affected even after 72 h of exposure to diatomite nanopowder concentration up to 300 μg/ml, thus confirming their usability as nanovectors in nanomedicine for therapeutic applications [31,32].

Functionalized diatomite nanoparticles were loaded with siRNA* using the same experimental protocol developed for microscopic frustules. H1355 cells were incubated with siRNA* modified diatomite nanoparticles (DNPs–siRNA*) to evaluate the siRNA uptake and cellular internalization. Fig. 11 shows a representative confocal microscopy image of cells treated with DNPs–siRNA* compared to untreated cells as control.

Fluorescence images show cell nuclei stained with Hoechst 33342 (blue) and cell membranes with WGA-Alexa Fluor 488 (green). Confocal microscopy analysis was performed after treatment with DNPs–siRNA* for 24 h. In Fig. 11 the presence of siRNA (labeled with Dy547, red) into the H1355 cells treated with DNPs–siRNA* is evident. Merge image reveals that siRNA molecules are localized in the cytoplasm of cells and no signals were observed inside the nucleus. Red fluorescence (siRNA*) was found as both spots and diffuse signal [27,33–35]. Efficiency of DNPs–siRNA* internalization was quantified by fluorescence microscopy: counting the number of red fluorescent cells and the total number of cells (determined in bright field), a ratio of about 75% was calculated.

3.4. Gene silencing

Finally, the ability of the DNPs–siRNA complexes to silence in H1355 cells targeted mRNA was investigated by Western blot analysis. In particular, a siRNA against glyceraldehyde 3-phosphate dehydrogenase (GAPDH) and a scramble siRNA as control were used. Moreover, to compare the efficiency of the DNPs–siRNA delivery system with that of other system, the commercially available Lipofectamine 2000 transfection reagent was used. The obtained results are reported in Fig. 12. Compared to untreated cells, GAPDH protein expression level after incubation of the cells with DNPs–siRNA complexes at 37 °C for 48 h was reduced (Panel A, upper gel) of about 22% (lane 2) as evaluated from the densitometric intensity of the bands (Panel B). Cells incubated with DNPs–SCR–siRNA (lane 3) showed instead almost identical protein expression level as control (lane 1), thus demonstrating the selective inhibition by siRNA. Panels C and D report the expression level and the densitometric analysis, respectively, of cells transfected with lipofectamine. In this case, GAPDH protein expression level (lane 2) was down-regulated of about 20%.

Even if the delivery efficiency of DNPs and lipofectamine 2000 is similar, the use of diatomite as nanocarrier is more suitable for medical applications since it allows: slow release of the loaded drug, loading with one or more different molecules (e.g. siRNA + drug), biocompatibility, and selective targeted functionalization to improve the delivery of antitumoral molecules to specific cell population.

4. Conclusions

The results of the presented work endorsed diatomite nanoparticles as innovative nanocarriers for siRNA transport in cancer cells. *In-vitro* toxicity studies highlighted the non-toxic nature of nanoparticles (average size less than 450 nm) up to 300 μg/ml concentration. An effective uptake of the engineered nanovectors into human epidermoid carcinoma cells, mainly localized in cytoplasm, was observed. Gene silencing in cancer cells by siRNA delivered by diatomite nanoparticles has been also demonstrated. Future perspectives regard the use of DNPs for iv delivery in *in vivo* applications.

Acknowledgments

The authors thank the DEREF S.p.A. for kindly providing the diatomite earth sample. The authors also thank S. Arbucci of the IGB-CNR Integrated Microscopy Facility for assistance with confocal microscopy acquisition, and G. Narciso of ICTP-CNR for EDS analysis. This work has been partially supported by Italian National Operative Program PON01 02782 and POR Campania FSE 2007–2013 (4-5), Project CRÈME.

References

[1] O. Şan, R. Gören, C. Özgür, Purification of diatomite powder by acid leaching for use in fabrication of porous ceramics, Int. J. Miner. Process. 93 (2009) 6–10.
[2] Y. Wang, J. Cai, Y. Jiang, X. Jiang, D. Zhang, Preparation of biosilica structures from frustules of diatoms and their applications: current state and perspectives, Appl. Microbiol. Biotechnol. 97 (2013) 453–462.
[3] R. Goren, T. Baykara, M. Marsoglu, A study on the purification of diatomite in hydrochloric acid, Scand. J. Metall. 31 (2002) 115–119.
[4] R. Goren, T. Baykare, M. Marsoglu, Effects of purification and heat treatment on pore structure and composition of diatomite, Br. Ceram. Trans. 101 (2002) 177.
[5] Q. Xiaohua, L. Mingzhu, C. Zhenbin, L. Rui, Preparation and properties of diatomite composite superabsorbent, Polym. Adv. Technol. 18 (2007) 184–193.
[6] E.M. Bens, C.M. Drew, Diatomaceous earth: scanning electron microscopy of Chromosorb P, Nature 216 (1967) 1046.
[7] M.J. Carter, I.D. Milton, An inexpensive and simple method for DNA purifications on silica particles, Nucleic Acids Res. 21 (1993) 1044.
[8] M.A.M. Khraisheh, M.A. Al-Ghouti, S.J. Allen, M.N. Ahmad, Effect of OH and silanol groups in the removal of dyes from aqueous solution using diatomite, Water Res. 39 (2005) 922–932.
[9] A.R. Parker, H.E. Townley, Biomimetics of photonic nanostructures, Nat. Nanotechnol. 2 (2007) 347–353.
[10] F. Xu, Y. Wang, X. Wang, Y. Tang, P. Yang, A novel hierarchical nanozeolite composite as sorbent fro protein separation in immobilized metal-ion affinity chromatography, Adv. Mater. 15 (2003) 1751–1753.
[11] J. Kim, P. Seidler, L.S. Wan, C. Fill, Formation, structure, and reactivity of amino-terminated organic films on silicon substrates, J. Colloid Interface Sci. 329 (2009) 114–119.
[12] L. De Stefano, A. Lamberti, L. Rotiroti, M. De Stefano, Interfacing the nanostructured biosilica microshells of the marine diatom *Coscinodiscus wailesii* with biological matter, Acta Biomater. 4 (2008) 126–130.
[13] L. De Stefano, L. Rotiroti, M. De Stefano, A. Lamberti, S. Lettieri, A. Setaro, P. Maddalena, Marine diatoms as optical biosensors, Biosens. Bioelectron. 24 (2009) 1580–1584.
[14] H. Zhang, M.A. Shahbazi, E.M. Mäkilä, T.H. da Silva, R.L. Reis, J.J. Salonen, J.T. Hirvonen, H.A. Santos, Diatom silica microparticles for sustained release and permeation enhancement following oral delivery of prednisone and mesalamine, Biomaterials 34 (2013) 9210–9219.
[15] M. Bariana, M.S. Aw, M. Kurkuri, D. Losic, Tuning drug loading and release properties of diatom silica microparticles by surface modifications, Int. J. Pharm. 443 (2013) 230–241.
[16] I. Ruggiero, M. Terracciano, N.M. Martucci, L. De Stefano, N. Migliaccio, R. Tatè, I. Rendina, P. Arcari, A. Lamberti, I. Rea, Diatomite silica nanoparticles for drug delivery, Nanoscale Res. Lett. 9 (2014) 329.
[17] L. Aagaard, J.J. Rossi, RNAi therapeutics: principles, prospects and challenges, Adv. Drug Deliv. Rev. 59 (2007) 75–86.
[18] K. Gavrilov, V.M. Saltzman, Therapeutic siRNA: principles, challenges, and strategies, Yale J. Biol. Med. 85 (2012) 187–200.
[19] K.A. Whitehead, R. Langer, D.G. Anderson, Knocking down barriers: advances in siRNA delivery, Nat. Rev. Drug Discov. 8 (2009) 129–138.
[20] W.X. Mai, H. Meng, Mesoporous silica nanoparticles: a multifunctional nano therapeutic system, Integr. Biol. 5 (2013) 19–28.
[21] S.A. Love, M.A. Maurer-Jones, J.W. Thompson, Y.S. Lin, C.L. Haynes, Assessing nanoparticle toxicity, Annu. Rev. Anal. Chem. 5 (2012) 181–205.

[22] Y.S. Lin, C.L. Haynes, Synthesis and characterization of biocompatible and size-tunable multifunctional porous silica nanoparticles, Chem. Mater. 21 (2009) 3979–3986.
[23] L. De Stefano, G. Oliviero, J. Amato, N. Borbone, G. Piccialli, L. Mayol, I. Rendina, M. Terracciano, I. Rea, Aminosilane functionalizations of mesoporous oxidized silicon for oligonucleotides synthesis and detection, J. R. Soc. Interface 10 (2013) 20130160.
[24] M. Terracciano, I. Rea, J. Politi, L. De Stefano, Optical characterization of aminosilane-modified silicon dioxide surface for biosensing, J. Eur. Opt. Soc. Rapid Publ. 8 (2013) 1303.
[25] S. Sorrentino, M. Naddeo, A. Ruso, G. D'Alessio, Degradation of double-stranded RNA by human pancreatic ribonuclease: crucial role of noncatalytic basic amino acid residues, Biochemistry 42 (2003) 10182–10190.
[26] P. Kumar, H. Wu, J.L. McBride, K. Jung, M.H. Kim, B.L. Davidson, S.K. Lee, P. Shankar, N. Manjunath, Transvascular delivery of small interfering RNA to the central nervous system, Nature 448 (2007) 39–43.
[27] F. Simeoni, M.C. Morris, F. Heitz, G. Divita, Insight into the mechanism of the peptide-based gene delivery system MPG: implications for delivery of siRNA into mammalian cells, Nucleic Acids Res. 31 (2003) 2717–2724.
[28] C. Chanéac, E. Tronc, J.P. Jolivet, Magnetic iron oxide–silica nanocomposites. Synthesis and characterization, J. Mater. Chem. 6 (1996) 1905–1911.
[29] A. Setaro, S. Lettieri, P. Maddalena, L. De Stefano, Highly sensitive optochemical gas detection by luminescent marine diatoms, Appl. Phys. Lett. 91 (2007) 051921.
[30] M.C. Morris, P. Vidal, L. Chaloin, F. Heitz, G. Divita, A new peptide vector for efficient delivery of oligonucleotides into mammalian cells, Nucleic Acids Res. 25 (1997) 2730–2736.
[31] R.E. Serda, J. Gu, J.C. Bhavane, X.W. Liu, C. Chiappini, P. Decuzzi, M. Ferrari, The association of silicon microparticles with endothelial cells in drug delivery to the vasculature, Biomaterials 30 (2009) 2440–2448.
[32] R.E. Serda, B. Godin, E. Blanco, C. Chiappini, M. Ferrari, Multi-stage delivery nanoparticle systems for therapeutic applications, Biochim. Biophys. Acta 1810 (2011) 317–329.
[33] S.W. Kim, N.Y. Kim, Y.B. Choi, S.H. Park, J.M. Yang, S. Shin, RNA interference *in vitro* and *in vivo* using an arginine peptide/siRNA complex system, J. Control. Release 10 (2010) 335–343.
[34] Y. Nakamura, K. Kogure, S. Futaki, H. Harashima, Octaarginine-modified multifunctional envelope-type nano device for siRNA, J. Control. Release 119 (2007) 360–367.
[35] A.M. Chen, M. Zhang, D. Wei, D. Stueber, O. Taratula, T. Minko, H. He, Co-delivery of doxorubicin and Bcl-2 siRNA by mesoporous silica nanoparticles enhances the efficacy of chemotherapy in multidrug-resistant cancer cells, Small 5 (2009) 2673–2677.